USGS
science for a changing world

Tephra from Kīlauea's 2008–2018 Lava Lake Eruption—Proximal Deposits and Dispersal Characteristics

Chapter D of
The 2008–2018 Summit Lava Lake at Kīlauea Volcano, Hawai'i

Professional Paper 1867

U.S. Department of the Interior
U.S. Geological Survey

Cover. Photograph showing the lava lake in the Overlook crater at Kīlauea Volcano, Hawai'i. The southeast sink is spattering in typical fashion. Tephra collection buckets labelled A8 and A8A are on the crater rim near the right edge of view, about 125 meters above the surface of the lava lake. Photograph taken by Don Swanson on February 28, 2014.

Tephra from Kīlauea's 2008–2018 Lava Lake Eruption—Proximal Deposits and Dispersal Characteristics

By Don Swanson, Tim Orr, Matthew Patrick, and Bruce Houghton

Chapter D of
The 2008–2018 Summit Lava Lake at Kīlauea Volcano, Hawai'i
Edited by Matthew Patrick, Tim Orr, Don Swanson, and Bruce Houghton

Professional Paper 1867

U.S. Department of the Interior
U.S. Geological Survey

U.S. Geological Survey, Reston, Virginia: 2026

Suggested citation:
Swanson, D., Orr, T., Patrick, M., and Houghton, B., 2026, Tephra from Kīlauea's 2008–2018 lava lake eruption—Proximal deposits and dispersal characteristics, chap. D *of* Patrick, M., Orr, T., Swanson, D., and Houghton, B., eds., The 2008–2018 Summit Lava Lake at Kīlauea Volcano, Hawai'i: U.S. Geological Survey Professional Paper 1867, 17 p., https://doi.org/10.3133/pp1867D.

ISSN 2330-7102 (online)

Acknowledgments

Kelly Wooten and Juanita Rause, volunteers at the Hawaiian Volcano Observatory, aided in sample collections early in the eruption, and Juanita made many observations and measurements of the enigmatic explosive deposit of April 16, 2008. Graduate students of Bruce Houghton (University of Hawai'i) helped with the mass per area measurements for several of the larger explosive deposits. Many Hawaiian Volcano Observatory volunteers and a few visitors accompanied Don Swanson on collecting rounds, adding excitement and discovery to the usual early morning walk. Sébastien Biasse (University of Geneva), Alexa Van Eaton (Cascades Volcano Observatory), and Kristi Wallace (Alaska Volcano Observatory) reviewed and markedly improved the manuscript. Kristi served as guest editor, because all editors of this Professional Paper volume are authors of this chapter.

Contents

Figures

Table

Conversion Factors

International System of Units to U.S. customary units

Multiply	By	To obtain
	Length	
centimeter (cm)	0.3937	inch (in.)
millimeter (mm)	0.03937	inch (in.)
meter (m)	3.281	foot (ft)
kilometer (km)	0.6214	mile (mi)
kilometer (km)	0.5400	mile, nautical (nmi)
meter (m)	1.094	yard (yd)
	Area	
square meter (m^2)	0.0002471	acre
square meter (m^2)	10.76	square foot (ft^2)
	Volume	
cubic meter (m^3)	6.290	barrel (petroleum, 1 barrel = 42 gal)
cubic meter (m^3)	264.2	gallon (gal)
cubic meter (m^3)	0.0002642	million gallons (Mgal)
cubic meter (m^3)	35.31	cubic foot (ft^3)
cubic meter (m^3)	1.308	cubic yard (yd^3)
cubic meter (m^3)	0.0008107	acre-foot (acre-ft)
	Flow rate	
meter per second (m/s)	3.281	foot per second (ft/s)
	Mass	
gram (g)	0.03527	ounce, avoirdupois (oz)
kilogram (kg)	2.205	pound avoirdupois (lb)
	Density	
kilogram per square meter (kg/m^2)	0.204816	pound per square foot (lb/ft^2)
kilogram per cubic meter (kg/m^3)	0.06242	pound per cubic foot (lb/ft^3)

Abbreviations

HST	Hawaii-Aleutian standard time
HVO	Hawaiian Volcano Observatory
m/a	mass per unit area
SE	southeast
USGS	U.S. Geological Survey
VEI	volcanic explosivity index

Tephra from Kīlauea's 2008–2018 Lava Lake Eruption—Proximal Deposits and Dispersal Characteristics

By Don Swanson,[1] Tim Orr,[1] Matthew Patrick,[1] and Bruce Houghton[2]

Abstract

A network of ten buckets was established early in the 2008–2018 summit eruption at Kīlauea to collect proximal tephra ejected from the new, informally named the "Overlook crater"; the buckets were emptied on most days of the eruption thereafter. This report summarizes the results of more than 2,400 different sampling intervals (most 1–3 days long) during the eruption, focusing on the physical and dispersal characteristics of the tephra deposits. The network was within about 300 meters south of the vent to capture tephra dispersed by the dominant northeast trade wind. The juvenile tephra mainly reflected spattering at the southeast (SE) sink, a downwelling area in the southeastern part of the lava lake in the Overlook crater that remained in the same area throughout the eruption, with admixtures of solid rock and secondary minerals derived from the wall of the crater. The proportion of juvenile material to lithic material ranged widely early in the eruption but was generally greater than 90 percent for the last 6 years of the eruption as lake level rose and the crater walls decreased in height and became more stable. The accumulation rate of tephra at each bucket was strongly dependent on the location of the bucket and reflects the interplay between lava lake level and wind direction and speed. The mass per unit area (m/a) of collected tephra was a maximum of about 97 kilograms per square meter for the entire eruption, equivalent to a thickness of about 75 millimeters. Thirty-two explosive events with a volcanic explosivity index of −2 to −4 deposited much of the tephra in the network. Fifteen of these rock-fall-induced events occurred within 6 days of one another. Pele's hair, a volcanic glass predominantly associated with quieter activity at the vent in the final half of the eruption, was dispersed more than 60 kilometers downwind from the lava lake and formed a nearly continuous deposit near the Overlook crater. This eruption was probably the most frequently sampled long-lasting eruption in history, but most of the deposits are ephemeral. The collected samples, although generally of small mass, are retained by the Hawaiian Volcano Observatory and are available for detailed study.

Introduction

Tephra was produced nearly every day of Kīlauea's 2008–2018 summit eruption in the "Overlook crater" (as it is referred to throughout this report), which is nested within the larger crater of Halemaʻumaʻu, in the southeast of the Island of Hawaiʻi. For most of the time during the eruption, the Overlook crater hosted a visible lava lake. Given the inaccessibility of the lava lake itself, with the enclosing crater wall that was vertical to overhanging, tephra that had reached the rim of Halemaʻumaʻu provided the only samples of quenched lava for most of the eruption. Systematic collection of this tephra (Swanson and others, 2009) afforded not only an inventory useful for assessing the chemical composition of the lava, but it also provided details about newly recognized dispersal characteristics, and hence eruption rates, in a proximal environment. Such detailed sampling was made possible by the rapid access to the rim of Halemaʻumaʻu from the Hawaiian Volcano Observatory (HVO). Buckets were deployed near the Overlook crater to collect tephra ejected from the lake. The network of buckets, and the tephra that fell in them, are described later in this chapter. All data used in this report are given in the data release published by Swanson and others (2026).

Shimano and others (2013) developed an automatic sampling device to collect ash at three remote sites on Sakurajima volcano in Japan, which still collects daily ash samples at the time of writing. We did not consider such an automatic device because we had to install buckets within 300 meters (m) of the vent to catch the usually sparse daily output—locations where particle size was commonly larger than ash size and where the collectors could be, and were, destroyed by larger explosions.

Wooten and others (2009) describe physical and chemical characteristics of ejecta from the eight explosions that punctuated the steady production of tephra from the Overlook crater in 2008. Houghton and others (2013) examine the dispersal characteristics and intensity of seven of the most powerful discrete explosions during the 2008–2018 eruption. Carey and others (2015) examine componentry from some of the early ash collected in buckets. Eychenne and others (2015) present and interpret detailed componentry data for two of the explosions in 2008. This paper does not attempt to duplicate that work.

[1]U.S. Geological Survey.

[2]University of Hawaiʻi at Mānoa.

Building on these previous studies, we focused only on tephra that fell within about 300 m of the vent, with exceptions for deposits of the larger explosions. Such proximal deposits formed from tephra that never reached more than a few hundred meters above the vent, generally much less. This tephra was subject to near-surface wind advection but not to processes that might affect higher plumes, such as rain scavenging. We did not study the sparse tephra deposits at medial and distal distances from the vent.

Installation and Management of Collecting Devices

Incandescent ejecta were observed coming from the newly opened vent on the evening of March 23, 2008, 4 days after the initial explosion on March 19. We established a systematic procedure to collect the tephra if pyroclastic eruptions continued. Around midday on March 25, 2008, nine aluminum roasting pans, each with a catchment area of 0.13 or 0.14 m^2 (square meters, depending on the brand of pan used), were placed on the ground near the crater to catch falling tephra. These sites, later named A1 through A9 (fig. 1), were chosen to sample the area in which tephra was falling consistently. For the next 6 days, we emptied the pans daily, often experiencing falling ash as we worked.

We quickly realized that the pans had two serious problems: (1) they were so light and had such a large surface area that the strong wind would blow them away and (2) there was little clearance to keep saltating ash reworked off the ground surface from contaminating the contents of a pan. Data acquired from the pans clearly showed that the mass accumulation rate of the tephra was high—in fact, probably far higher than at any time during the 10 years of eruption except during transient discrete explosions—but the quality of the samples is poor because of contamination. Thus, the data obtained by the pans are only used qualitatively in this study.

On April 1, 2008, the pans were replaced with plastic paint buckets that had two advantages. The top of each bucket was about 25 cm above the ground surface, thereby reducing contamination by wind reworking, and they were heavy enough to withstand strong wind once a weight was placed in each bucket. These nine buckets, augmented by a tenth bucket called A8A (placed on a fence near bucket A8 on May 13, 2008), formed the tephra-collecting array for the rest of the eruption (fig. 1). The catchment area of each bucket ranged from 0.057 to 0.042 m^2, depending on which brand of bucket was used; for the last several months of the eruption, all buckets were of the same brand and had a catchment area of 0.042 m^2.

A ring of rocks surrounded each bucket, forming a nest that helped to keep the bucket in place during strong winds. The metal handle was removed from each bucket before installation in the field, because the handles corroded in the acidic environment and would shed metal flakes into the bucket, causing contamination. Each bucket was replaced as needed during the 10 years, owing to gradual deterioration and, for some, partial melting by hot lapilli. It is important to note, however, that the locations of the buckets did not change after their initial deployment. This allowed direct comparisons among data acquired at any time during the 10-year eruption.

Tephra-Collection Procedure

The buckets were emptied each weekday or more often if eruptive conditions warranted it. The roundtrip walking route from the parking lot (fig. 1) was slightly longer than 1 kilometer (km), and buckets were generally emptied in reverse numerical order on each trip; bucket A9 was first and bucket A1 was last. Collecting took about 35 minutes and was usually done just before dawn, so that the results could be incorporated into HVO's morning update, if appropriate. Therefore, tephra collected on a particular morning mostly fell on the previous day; this is important when correlating the mass of tephra collected with one or more specific events. Starting in late July 2013, laser rangefinder measurements to the surface of the lava lake were made during each collecting trip from sites near buckets A8A and A4, adding several minutes to the overall routine. The rangefinder measurements were used to document the changing level of the lava lake.

In the field, the contents of each bucket were poured, with the aid of a brush and plunger, through a funnel into a small plastic bag labeled with the location, time, and date. In the laboratory, the contents of each bag were dried (if necessary) and weighed to the nearest 0.01 gram (g). The accumulation rate was calculated on a spreadsheet—the hourly rate at which tephra collected in a bucket—for the period of time between collection, and an average accumulation rate for the entire network was calculated for all 10 buckets. The average wind speed for the period from the start of one collection to the start of the next—usually about 24 hours—was calculated, using an anemometer near HVO in order to evaluate the effect of wind speed on tephra accumulation rate.

The tephra from one bucket, typically bucket A7, was sieved into grain sizes larger and smaller than 0.5 millimeters (mm) in diameter. The >0.5-mm-size portion was then examined under a binocular microscope and separated into juvenile and non-juvenile components (wall-rock lithic fragments and secondary alteration products [mostly anhydrite], respectively) that were separately weighed to the nearest 0.0001 g and bagged. The weight percentage of juvenile components was then calculated to further characterize the tephra.

Effect of Wind

Wind speed and direction were routinely measured at 15-minute intervals during the eruption (fig. 2). The average speed throughout the entire eruption was 4.8 meters per second (m/s).

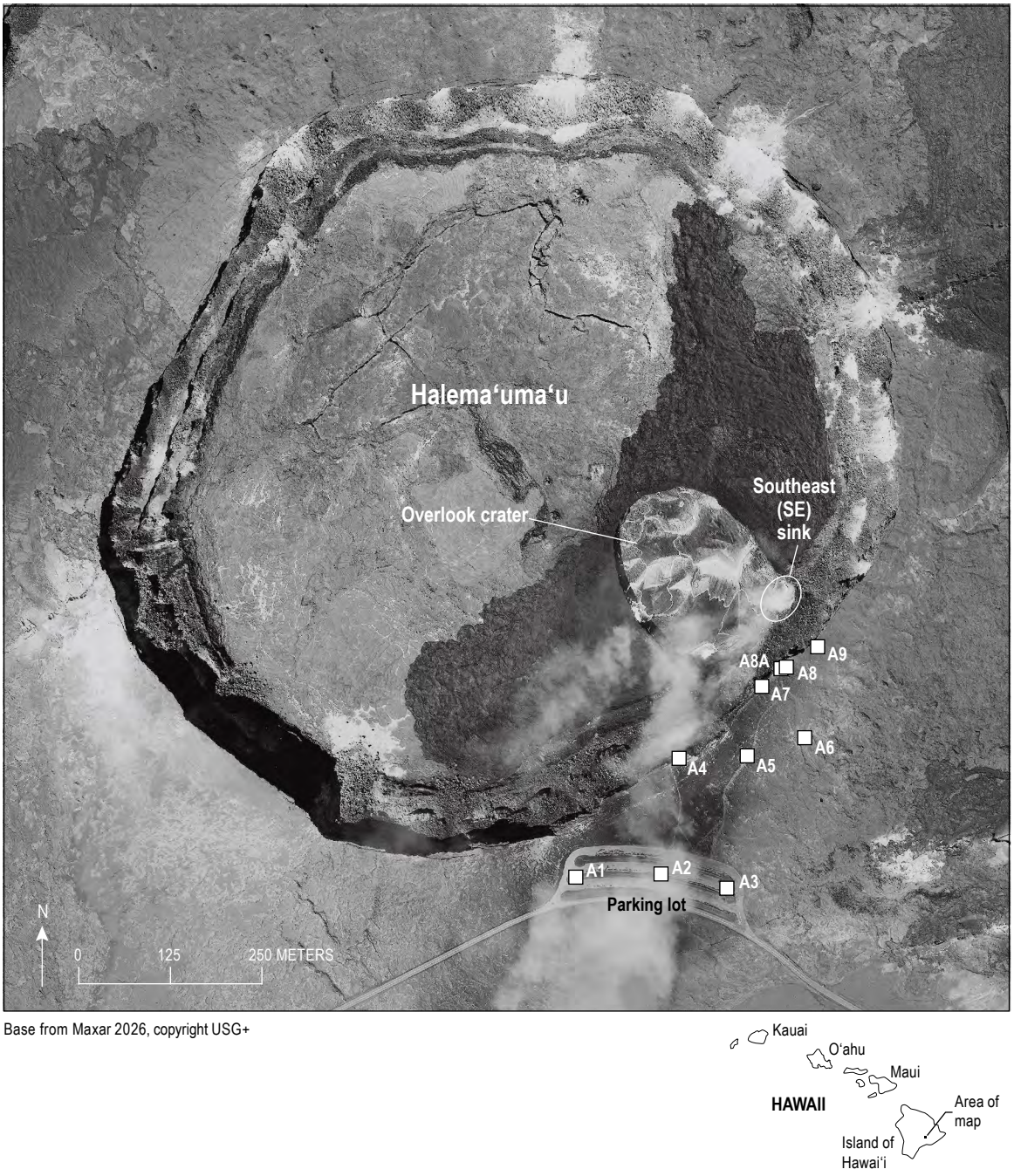

Figure 1. Map showing locations of buckets (labeled A1 through A9) for collecting tephra, unchanged during the 10 years of eruption (2008–2018) at the summit of Kīlauea, Island of Hawai‘i. In this view from 2016, a lava lake occupies the Overlook crater. Dark areas on the floor of the Halema‘uma‘u crater are lava flows that spilled from the Overlook crater in 2015.

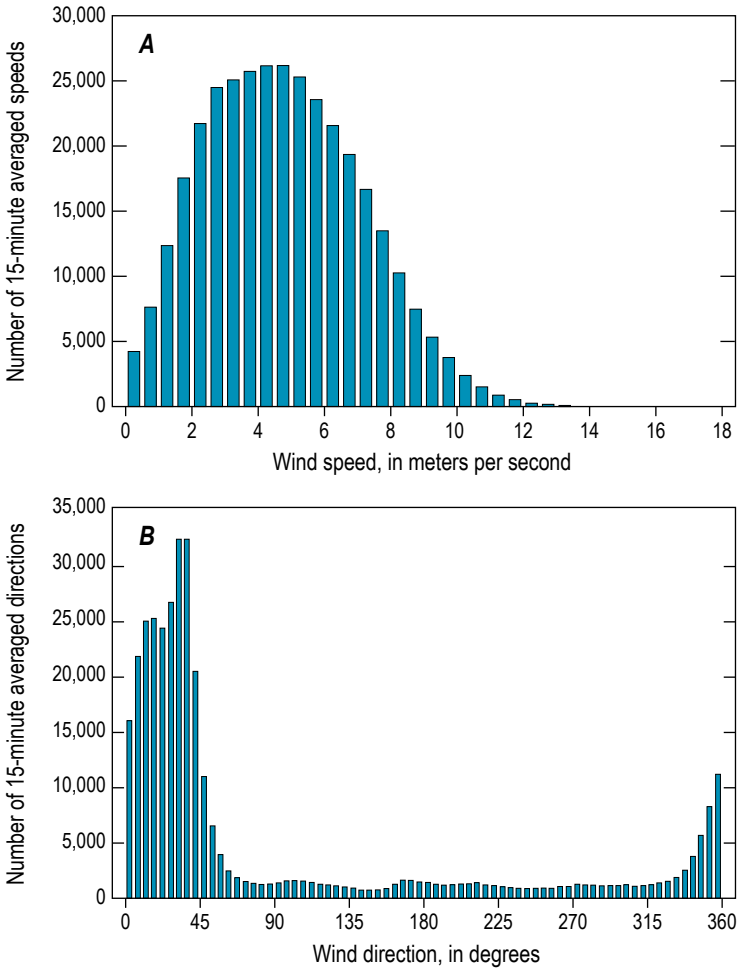

Figure 2. Plots showing wind speed, *A*, and wind direction, *B*, for the entire eruption, measured in 15-minute intervals at the Hawaiian Volcano Observatory. Bin size in *A* is 0.5 meters per second (m/s); in *B*, the bin size is 5 degrees. Dominance of northeast wind, or trade wind, direction is evident in *B*. Average wind speed is 4.8 m/s for the 344,886 total measurements, shown in *A*.

The northeast wind direction, or trade winds, dominated in frequency; the south wind, or Kona winds, was comparatively infrequent. Until July 14, 2011, the wind speed and direction were recorded by an instrument at HVO; thereafter, the data were also recorded from an instrument at North Pit, on the north rim of Halemaʻumaʻu. Both instruments recorded similar wind speeds and directions, although the North Pit instrument typically recorded slower wind speeds (0.1–0.4 m/s) than the HVO instrument, but the readings could be variable. Because of the comparable data, the two wind gages provided a consistent dataset throughout the ten years of the eruption. For the sake of uniform data, figure 2 shows data sourced from the instrument at HVO.

Wind speed was compared with tephra accumulation rate to test the hypothesis that the accumulation rate would vary with wind speed. There was little effect of the wind speed on the average network accumulation rate (fig. 3*F*). However, the wind speed affected the accumulation rate at individual buckets in an unanticipated way. Buckets A1 and A4, downwind during the trade winds, show a peak in accumulation rate at a wind speed of about 5 m/s (figs. 3*A*, *B*). Seemingly, slower speeds are less able to transport tephra (mostly ash) to the buckets, and faster speeds tend to carry the ash past the buckets. Bucket A8A shows a similar pattern, although the peak accumulation rate is lower because of a slightly lower wind speed (fig. 3*C*). The wind effect was minor or absent at bucket A7 (fig. 3*D*), which was almost directly above the southeast (SE) sink, an area of downwelling against the southeastern crater wall that remained throughout the eruption. Bucket A7 most likely collected tephra supplied directly by the thermally buoyant plume above the sink before it was advected away by the wind.

Bucket A9, upwind from the spattering sites during trade winds, shows a different pattern (fig. 3*E*). Many of the low wind speeds were during the Kona winds, so the accumulation rate was highest at such times. The stronger winds were typically trade winds, and the accumulation rate decreased accordingly as increasing speed more efficiently transported ash away from bucket A9.

To our knowledge, this is the first time that such detailed influences of wind speed on transport and deposition of ash have been recognized, at least in a proximal setting. The effects are apparent because of the long duration of the eruption, the presence of local wind gages, and the repeated production of tephra by weak spattering during a variety of wind speeds. However, there is still uncertainty whether stronger fountaining and ash plumes with more convection would have experienced similar wind effects on a medial or distal spatial scale.

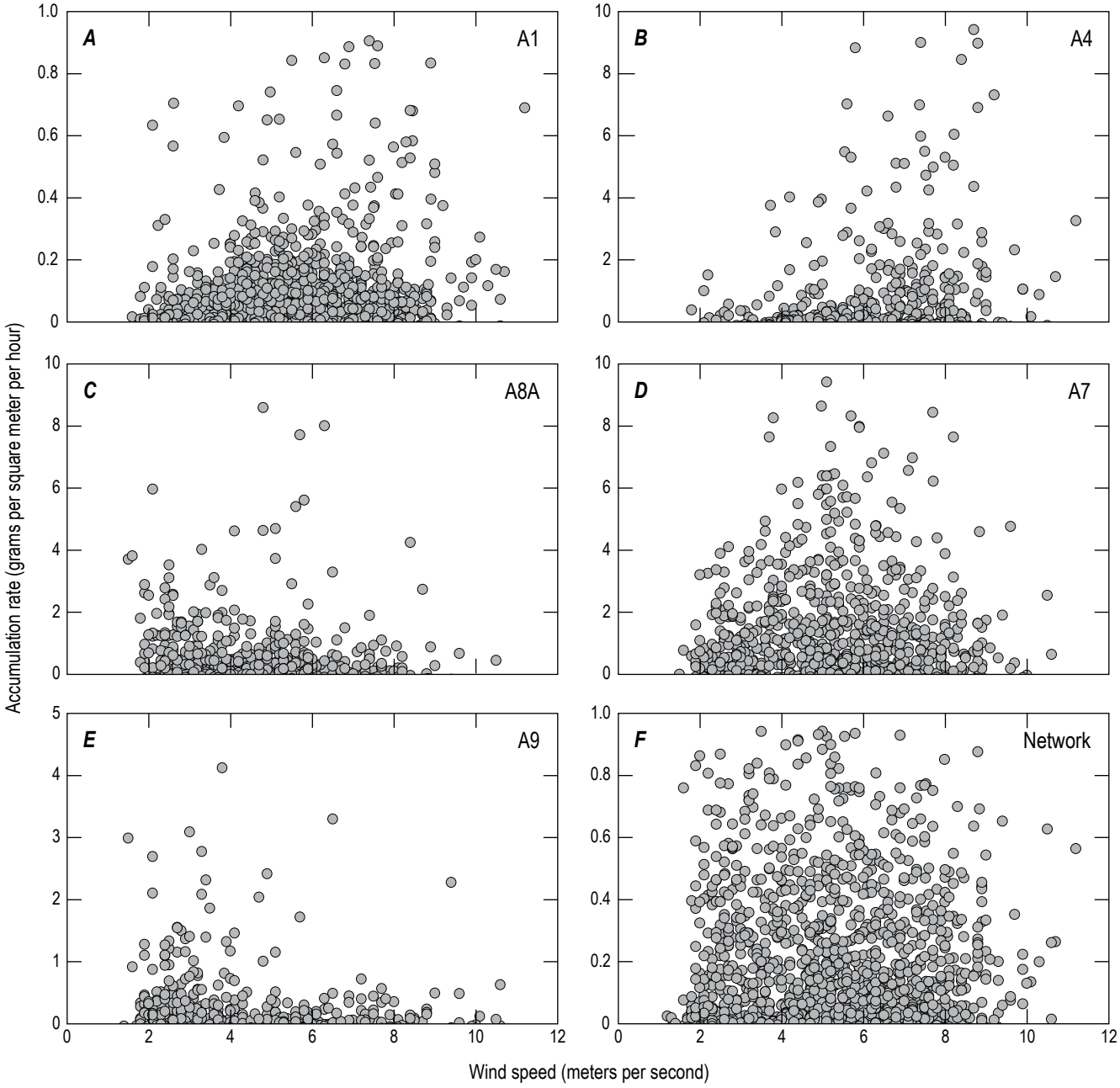

Figure 3. Graphs showing effect of wind speed on accumulation rates of tephra in five buckets and across the entire network. Buckets A1 (*A*) and A4 (*B*) tended to collect more tephra at wind speed of 5–6 meters per second. *C*, Bucket A8A showed a similar pattern but at a slightly lower wind speed. *D*, The accumulation rate in bucket A7 was affected slightly, if at all, by wind speed. *E*, Upwind bucket A9 collected more tephra when wind speed was low. *F*, The average accumulation rate for the entire network was little affected by wind speed.

Accumulation Rates at Buckets A4 and A7

Throughout the eruption, buckets A4 and A7 typically acquired the most tephra on a day-to-day basis. Figure 4 shows that A4 contained the most tephra more than 860 times, and A7 more than 960 times, totaling more than 1,820 times out of the approximate 2,400 collections; buckets A8, A8A, and A9 accounted for most of the remaining approximate 580 collections. Bucket A4 was directly down the trade wind direction from the south end of the lava lake, and bucket A7 was directly above the south end. Accordingly, it is not surprising that these two buckets generally acquired the most tephra mass.

Buckets A4 and A7 each accounted for most of the collected tephra mass but at different periods during the eruption, likely reflecting changing conditions within the

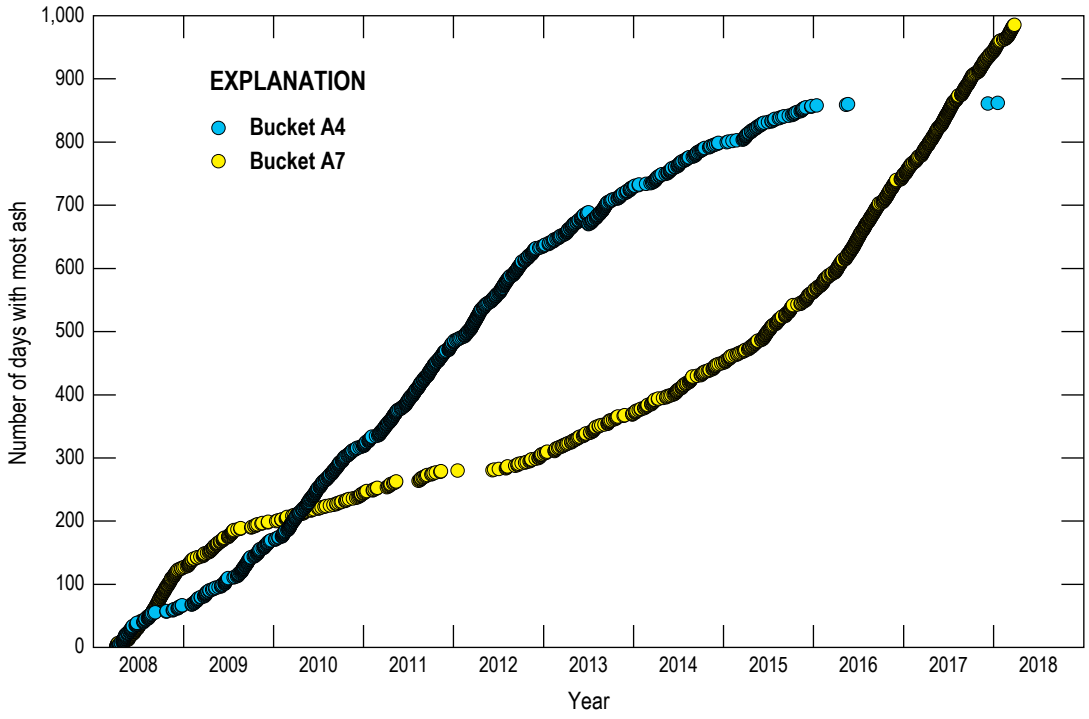

Figure 4. Graph showing the cumulative number of times that buckets A4 and A7 contained more tephra than any other bucket in the network.

Overlook crater (fig. 4). Until late 2012, the lava lake within the Overlook crater was either absent or very deep and only sporadically visible. Rockfalls were numerous during this time, and trade winds blew mostly lithic ash that fell into bucket A4. Fairly little convective thermal updraft reached the rim of Halemaʻumaʻu when the lake surface was low, so bucket A7, directly above the widening crater, received little ash compared to bucket A4. From late 2012 onward, however, the lake level was sufficiently high enough that spattering could often send juvenile ash into bucket A7, largely carried by the convective thermal updraft, especially above the SE sink. As a result, the daily amount of juvenile mass collected in the network slowly rose in 2013–2015 before increasing by several times in 2016 with rising lake level, particularly accumulating in A7. Tephra fall continued at bucket A4 in 2016, but it was mostly juvenile and much less abundant than at A7. Mintz and others (2021; chap. E of this volume) describe the nature of spattering in early 2015, and such activity characterized the SE sink during the later high stand of the lava lake.

Juvenile Percentage of Tephra During the Eruption

Large changes in tephra componentry with time characterized the decade-long eruption (fig. 5). These changes are defined by the proportions of juvenile components (Pele's hair and tears, hollow spherules, and bubble walls) and lithic components (clasts derived from the wall of the Overlook crater and secondary alteration minerals, chiefly anhydrite). The changes mainly reflect different levels of lava in the lake and the interaction of the lava column with the wall of the crater.

Starting in 2018, the juvenile component percentage each day was generally greater than 98 percent, whereas all the ash was lithic on some days during the first 4 years of the eruption. The juvenile to lithic proportions ranged widely during the first 2 months of the eruption, reflecting the continued deep level of lava and the repeated rock falls from the overhanging crater wall. The rock falls produced fine debris that fell onto the lake surface and were incorporated into the spattering from the lake.

The juvenile proportion began to gradually increase, from 20 to 50 percent in early June 2008 to 60 to 90 percent by late November 2008. The first view of the lava lake was on September 5, 2008 (Patrick and others, 2021; chap. A of this volume), perhaps indicative of a rising lava level during the summer that was responsible for the increasing juvenile component percentage. The crater widened during this time, contributing more wall-rock clasts to the erupted tephra.

The juvenile to lithic component ratio plummeted starting in early December 2008, as lake level withdrew (Patrick and others, 2021; chap. A of this volume), bottoming at 0 percent on December 8 and remaining less than 10 percent until February 4, 2009. The volume of ash was small during these two months and may have been mainly rock-fall dust wafted from the crater by thermal updrafts.

After this two-month period, the juvenile to lithic ratio gradually increased, and by May–June 2009 it was up to 70 to 90 percent (fig. 5). This period resembles that of summer and fall 2008, as the lake level was probably rising and able to contribute more spatter to the rim of Halemaʻumaʻu. Similar to 2008, this 2009 period ended abruptly on June 30 with withdrawal of the lake, and for the next 4.5 months few juvenile

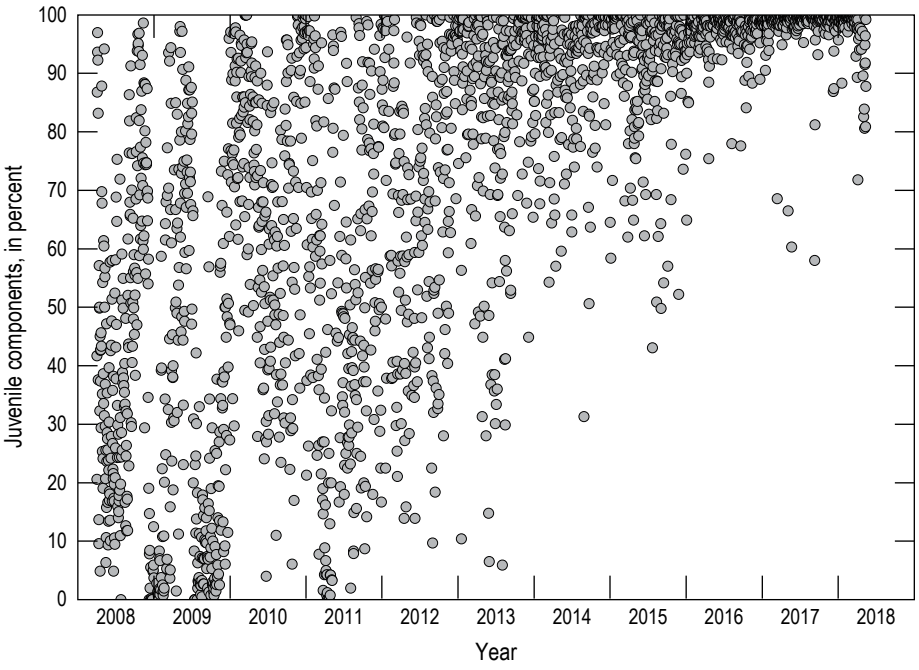

Figure 5. Graph of juvenile components (in percentage) versus time during the 2008–2018 Kīlauea eruption. The explosions listed in table 1 are excluded.

components were collected relative to the previous months, with a juvenile to lithic ratio generally less than 40 percent. The surface of the lava lake was deeper than previously measured, however, and only sporadically increased to higher ratios, most notably on September 17, 2009, when the juvenile to lithic ratio reached nearly 70 percent.

In late 2009, the juvenile to lithic ratio increased again and remained greater than 70 percent until June 2010 before decreasing to 30 to 60 percent for the next 3–4 months. Afterward, the ratio varied widely into 2011, lowering to <10 percent in March during the Kamoamoa fissure eruption (March 5–9, 2011) (Patrick and others, 2021; chap. A of this volume) when the lake level dropped, and it remained low through April. Thereafter, the lake level began a slow rise, and the juvenile to lithic ratio followed suit, with notable reversals, continuing through to the end of the eruption in 2018.

The increase of juvenile components after 2011, particularly in 2012, is striking and had at least three causes. The main cause was rising lava lake level; the development of the consistently high-level lake starting in late 2012 brought sites of spattering closer to the rim of Halemaʻumaʻu, resulting in more juvenile tephra falling into the bucket network (fig. 6). Thus, the juvenile percentage increased without a need to decrease the amount of nonjuvenile tephra in the buckets. This is particularly evident starting in late 2015 but is apparent between 2012 and 2015 as well (fig. 6).

Two other causes of increasing juvenile proportion are minor but still noteworthy. One is that the drowning of the crater wall by rising lake level made less wall material available to supply lithic material to the tephra. This leads to an absolute loss in the lithic components. The other cause is that the crater wall above the lake was gradually stabilizing. For the first several years of the eruption, much of the wall, especially around the northern part of the Overlook crater, was overhanging and, hence, unstable. With time, most of the overhang was lost through rock falls, so there was less lithic material that could fall directly into the lake and be erupted as tephra.

The most noticeable increase in collected juvenile mass took place over about a 2-month period in December 2015 and January 2016 (fig. 6). At that time, lake level rose from a 2-year (2014–15) average elevation of 977 m to a 2-year (2016-17) average of 1,000 m. This 23-meter rise shortened the average depth between the spattering sites and the rim of Halemaʻumaʻu from 131 to 108 m. That 23-meter change accompanied more than a sixfold increase in the average daily collected juvenile mass from 0.7 grams per day (g/d) in 2014–15 to 4.5 g/d in 2015–16. The SE sink was the principal spatter site throughout this four-year period, so that the increase in collected juvenile mass cannot be ascribed to shifting spattering locations. Instead, it must reflect either an increase in the gas content—and therefore explosivity—of the magma or the shorter vertical distance needed for the convective thermal plume above the SE sink to deposit ash and smaller lapilli onto the rim of Halemaʻumaʻu.

Lacking evidence to the contrary, it seems most likely that the 23-meter decrease in vertical distance allowed the convective plume to lift more than six times the amount of juvenile tephra onto the rim and into the collecting buckets. Mueller and others (2018) demonstrated the importance of wall height in governing if tephra left the Kīlauea Iki vent in 1959, where a high wall trapped tephra within the crater. The Halemaʻumaʻu eruption provides a small-scale example of such topographic control on tephra dispersal.

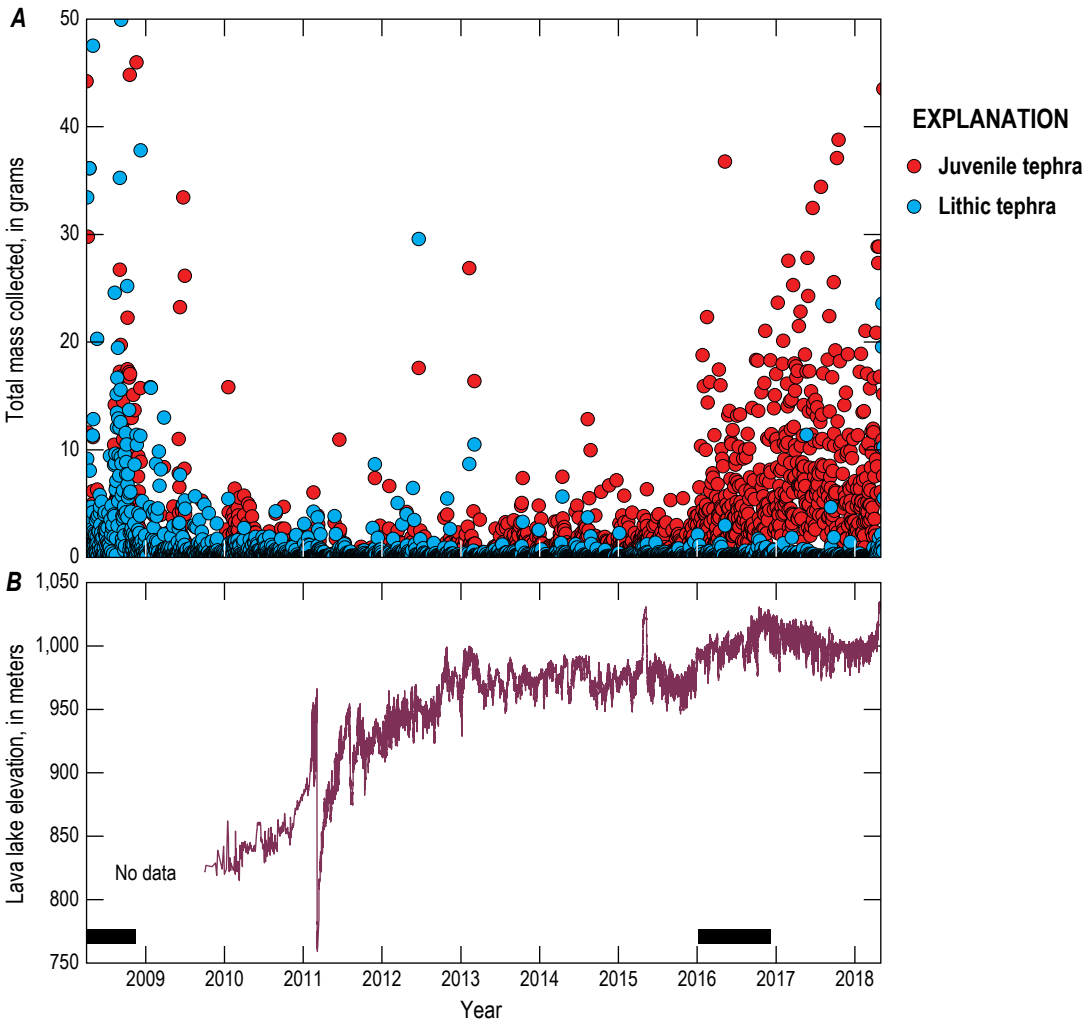

Figure 6. *A*, Graph showing the total mass of juvenile and lithic tephra collected nearly daily from the complete bucket network during the 2008–2018 Kīlauea eruption. Data spans from April 1, 2008, to May 1, 2018. The explosions listed in table 1 are excluded. *B*, Surface elevation of the Outlook crater lava lake as automatically measured since September 30, 2009 (Patrick and others, 2021; chap. A of this volume). Bars at bottom of figure indicate two periods in 2008 and 2016 of frequent, large explosions (table 1).

Amount of Tephra Collected

Small amounts of tephra, mostly composed of ash but including rare lapilli (Pele's tears and small fragments of pumice) rarely more than 10 cm long, were collected from the buckets. For the first eight years of the eruption, it was uncommon for a bucket to contain more than 1 g after 24 hours of deposition. Starting in 2016, however, the tephra accumulation rate was much higher; at least one bucket would contain several grams, and two to three other buckets might have had 1–2 g after 24 hours.

The catchment areas of the buckets, and the amount of tephra that could be collected, varied with time. To facilitate comparisons, a mass per unit area value (m/a), generally expressed as grams per square meter, was calculated from the collected amount in each bucket. All tephra masses and thicknesses in this paper are based on such m/a values unless otherwise noted.

Figure 7*A* shows the 10-year m/a totals for the ten buckets, not counting fallout from rockfall-induced explosive events. Isomass contours based on m/a values are drawn in the figure. Bucket A7 collected the equivalent of 68.2 kilograms per square meter (kg/m^2), nearly double the amount in bucket A4 (35.3 kg/m^2). Buckets A8 and A8A collected smaller amounts than bucket A4 despite being nearer the SE sink. Bucket A4 most likely collected ash that rose high enough convectively to have been advected by the trade wind, whereas buckets A8 and A8A received mostly ash that barely rose out of Halema'uma'u. Bucket A7 is favorably located to receive tephra from wind advection and from the lower part of the convection thermal updraft above the spattering sink.

Using an assumed deposit density of 1,300 kilograms per cubic meter (kg/m^3) (a common deposit density for fine-grained pyroclastic deposits; Houghton and others, 2013), a cumulative

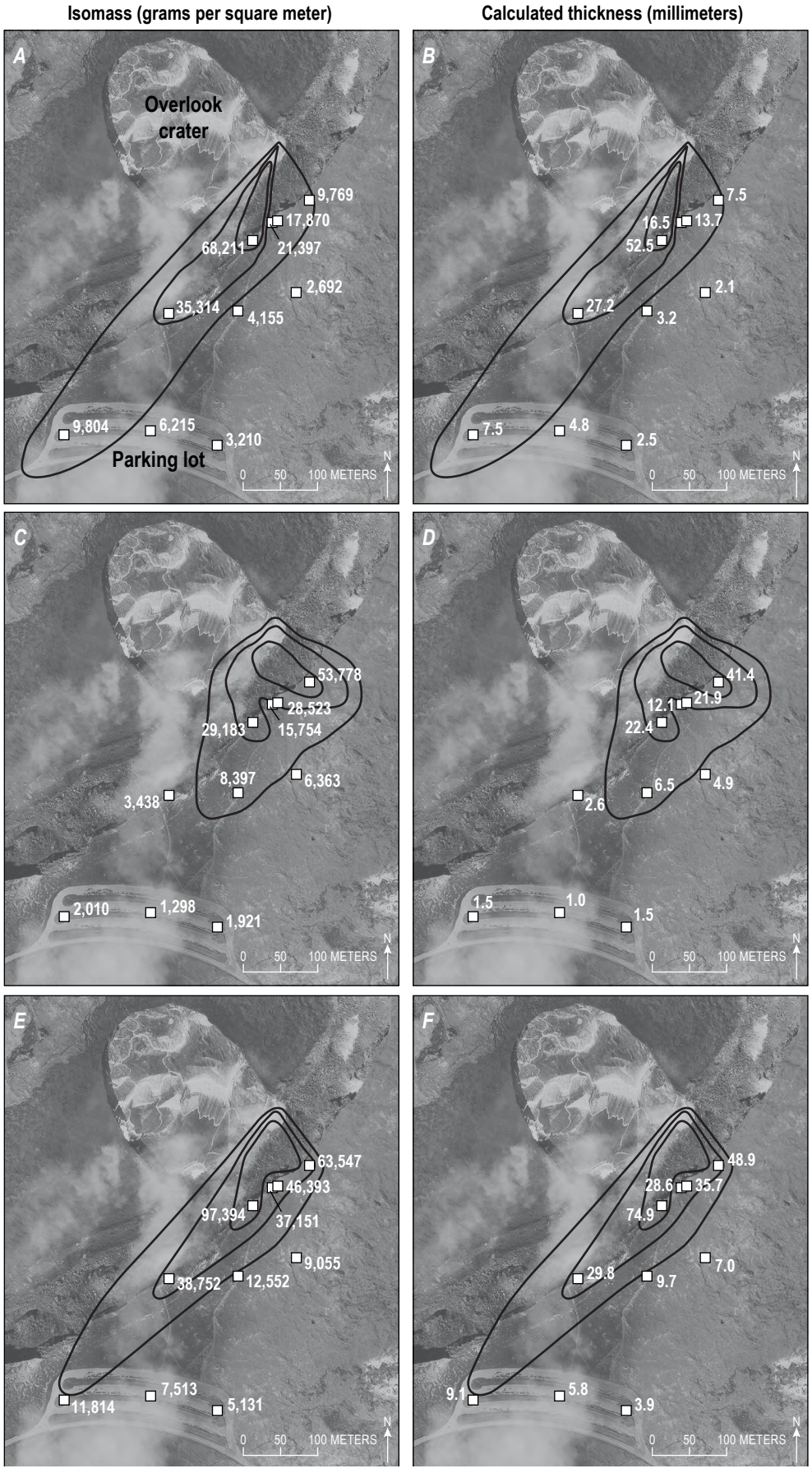

thickness (T_{1300}) of tephra at each bucket site can be calculated (fig. 7*B*). Values range from about 53 mm at bucket A7 down to 2 mm at bucket A6. Such thicknesses do not match observed total thicknesses, however, because of erosion throughout the 10 years and the fact that Pele's hair forms a highly inflated deposit with a deposit density much less than 1,300 g/m^2; for example, Pele's hair accumulated around bucket A7 to a measured uncompacted thickness of more than 20 cm during 2016–17.

Thirty-two rockfall-induced explosive events (Orr and others, 2013) deposited bombs or blocks outside Halema'uma'u (table 1). The first and largest event initiated the eruption on March 19, 2008, before the bucket network was installed (Houghton and others, 2011, 2017). Values of m/a for the 31 later explosive events are shown in figure 7*C*. Bucket A9 had an m/a value of about 53.8 kg/m^2, almost double the value at bucket A7. This reflects the largest spatter fall of the eruption outside of Halema'uma'u on August 6, 2016; it was directed toward

Figure 7. Maps of mass per unit area (m/a; in grams per square meter) and calculated thickness (in millimeters) for tephra collected in the bucket network for the entire eruption (2008–2018) after April 1, 2008. *A*, Isomass contours for m/a values excluding the 31 explosive events. *B*, Calculated thickness for the m/a values in part *A*. *C*, Isomass contours for the 31 explosive eruptions after April 1, 2008. *D*, Calculated thickness for the m/a values in part *C*. *E*, Isomass contours for all tephra collected in the buckets, the sum of the m/a values in parts *A* and *C*. *F*, Calculated thickness for the m/a values in *E*.

Table 1. Juvenile component percentage, volume, and volcanic explosivity index for the 32 rockfall-induced explosive events of the 2008–2018 Kīlauea eruption.

[Dates shown as month/day/year. %, percent; m^3, cubic meter; —, not applicable]

Date of event	Juvenile component (%)	Volume (m^3)	Volcanic explosivity index
03/19/2008	0	310[a]	−2
04/09/2008	14	100[a]	−2
04/16/2008	5	—	—
08/01/2008	39	10[a]	−3
08/27/2008	52	16[a]	−3
09/02/2008	86	210[a]	−2
10/12/2008	94	43[a]	−3
10/14/2008	97	9[a]	−4
09/17/2009	69	—	—
04/26/2010	74	—	—
01/17/2011	46	10	−3
01/21/2011	53	—	—
12/21/2011	97	—	—
02/03/2012	94	—	—
08/23/2013	92	15	−3
07/23/2014	81	15	−3
10/19/2014	98	8	−4
04/25/2015	94	—	—
04/28/2015	94	17	−3
05/03/2015	85	1	−4
01/02/2016	65	—	—
01/08/2016	94	17	−3
04/19/2016	75	10	−3
08/06/2016	78	72	−3
09/19/2016	78	4	−4
10/19/2016	92	5	−4
10/20/2016	94	27	−3
11/28/2016	96	3	−4
12/02/2016	99	4	−4
01/19/2018	88	30	−3
04/06/2018	72	59	−3
05/09/2018	95	230	−2

[a]Houghton and others (2013).

bucket A9, resulting in a measured m/a value of 49.8 kg/m^2, which is 85 percent of the 10-year total m/a value for that bucket. The 2016 explosion produced a T_{1300} of 41 mm at bucket A9 (fig. 7*D*).

Figures 7*E* and 7*F* show the 10-year m/a and T_{1300}, respectively, for all the tephra collected in the buckets, including that deposited during explosive events. Bucket A7 netted the most tephra, about 97.4 kg/m^2 with a T_{1300} of 75 mm. Bucket A3 acquired the least amount of tephra, about 5.1 kg/m^2 and a T_{1300} of 4 mm.

Figure 8 illustrates varying patterns of tephra accumulation. Steps in the curves result from rockfall-induced explosive events. The m/a accumulation rate in 2008 was high at buckets A4 and A7 but not at A9, which was usually upwind of the lake (fig. 8). Starting in 2009, the accumulation rate was faster at A4 than A7 and was rather steady thereafter. The accumulation rate began picking up at A7 in early 2016, as lake level rose and the convection thermal updraft could carry tephra high enough to reach A7. The accumulation rate at A9 began to increase at about the same time but was greatly offset by the explosive event of August 6, 2016.

The m/a accumulation rates at buckets A8 and A8A are broadly similar to one another (fig. 8). The buckets are 7 m apart; A8 is at an azimuth of 75 degrees from A8A and about 3 m farther from the rim of Halemaʻumaʻu. The small difference in location leads to slightly higher accumulation rates at bucket A8A. We originally installed A8A on a fence post 110 cm above ground to test the theory that wind reworking would increase the apparent accumulation rate at A8 (and at all buckets on the ground). Instead, the data show that reworking is a minor concern and that the position of A8A slightly closer to the spattering site controls the difference in accumulation rates. As illustrated by these buckets, tephra accumulation rate in a near-vent setting depends on location.

The amount of tephra that fell into the bucket network probably constituted only a small portion of all the tephra produced during the eruption. A substantial but unquantified amount fell onto the floor of Halemaʻumaʻu, inaccessible to study except for one brief visit by helicopter in 2016. Spattering took place from ephemeral sites around the periphery of the lava lake and frequently deposited tephra on the floor of Halemaʻumaʻu, well below the elevation of the bucket network. For example, the floor of Halemaʻumaʻu was generally less than 60 m above the lake before May 2015 (when it overflowed, it raised the rim by 8 m) and generally less than 30 m after 2016. In contrast, the bucket network was about 85 m above the floor of Halemaʻumaʻu. Consequently, much of the tephra produced by spattering was trapped within Halemaʻumaʻu, most falling back into the lava lake, but some deposited on the floor of Halemaʻumaʻu and on the sloping wall above the southeastern end of the lake.

Because so much tephra was inaccessible, the tephra collected in the buckets is not an accurate gage of the total tephra production from the Overlook crater. It is instead a minimum measure of the output from the SE sink area, which was the most persistent site of downwelling in the lava lake and the most frequent site of spattering in the later years of the eruption. The varying accumulation rate of tephra in the network broadly reflects other observed changes, too; specifically, the level of lava in the lake and subtle changes

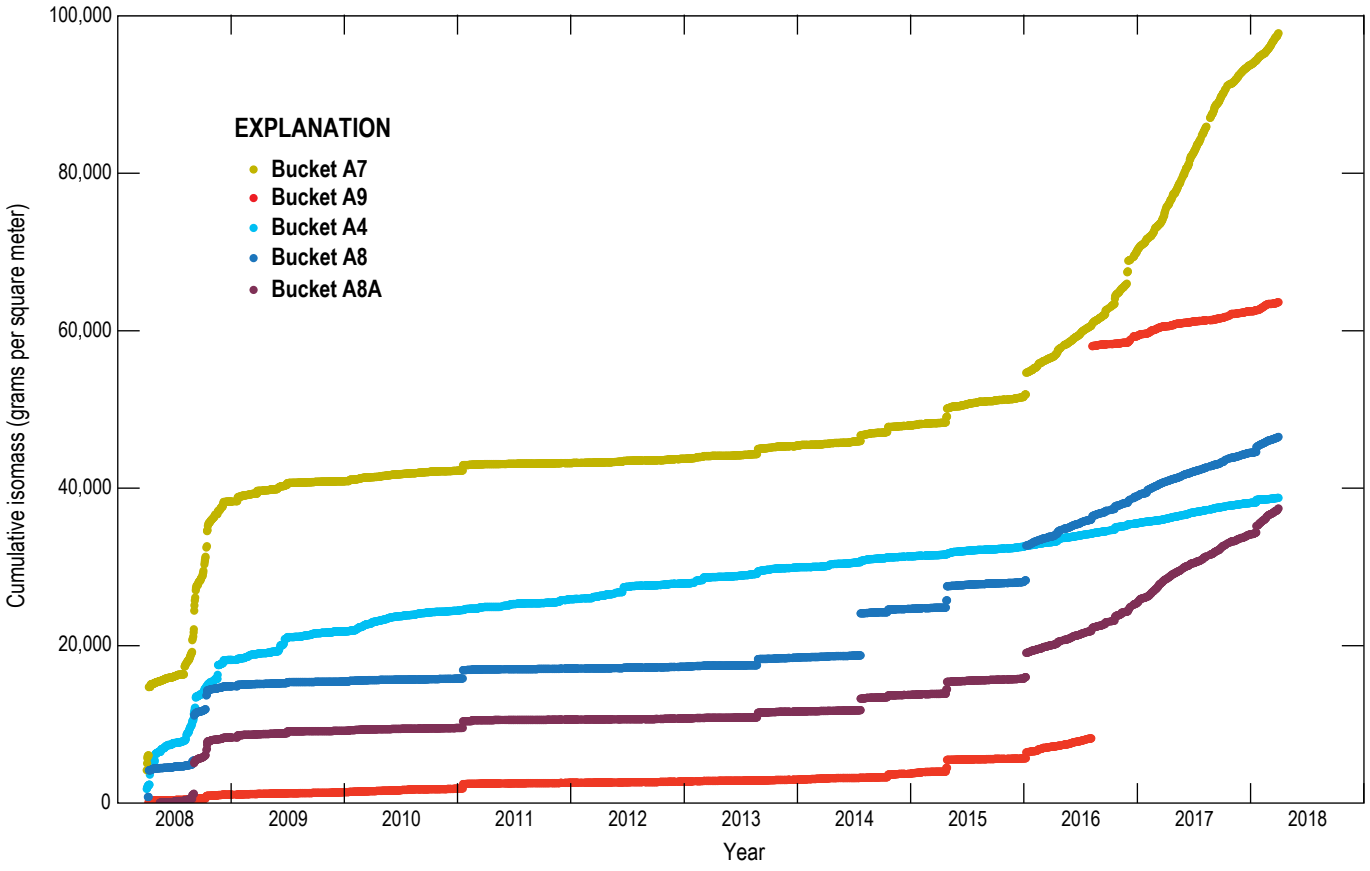

Figure 8. Plot of cumulative mass per unit area (m/a) (in grams per square meter [g/m^2]) for selected individual buckets spanning the entire eruption after April 1, 2008, to May 2018. Offsets in curves indicate sudden tephra accumulation during explosive events.

in elevation of the summit area measured by Global Position System (GPS), both probably resulting from a pulsing magma supply (Swanson and others, 2017).

Distribution of Pele's Hair

Pele's hair mainly accumulated between the Overlook crater and the Halemaʻumaʻu parking lot, where it formed a nearly continuous loose blanket and local drifts. It was common to feel Pele's hair falling on one's face; the sensation was like walking through a cobweb, and one would invariably try to brush the hair away. First-time visitors in the Halemaʻumaʻu parking lot were always amazed by the drifts of Pele's hair along the curb, and many found out the hard way that a handful of Pele's hair left glassy, needlelike shards prickling their hands.

However, Pele's hair was not confined to the summit area; it was also dispersed far downwind, falling as far as Hawaiian Ocean View Estates, 60 km southwest of the lava lake. The ground surface within several kilometers south of the lava lake had a discontinuous coating of Pele's hair (fig. 9*A*), and drifts of loose hair 20–30 cm thick collected downwind of obstacles (fig. 9*B*, *C*). With a low sun angle, the surface deposit presented an amber sheen when looking toward the sun, but a dull brown shade when looking away.

The deposits of Pele's hair formed over the course of the eruption but especially thickened during the final three years when the lake level was high and tephra accumulation rates soared (fig. 10). In addition, some explosive events themselves produced large amounts of Pele's hair, sometimes creating overnight a pristine fluffy deposit akin to newly fallen snow.

When the southern Kona wind was blowing, Pele's hair fell north of the caldera in neighboring residential areas, never accumulating into continuous deposits but leaving individual filaments glistening in the sun. Two trees at HVO were sometimes decorated with strands of Pele's hair 10–20 cm long that resembled tinsel on a Christmas tree.

The presence of Pele's hair south of the Kīlauea caldera guided the interpretation of a similar deposit that accumulated there in the early 19th century. Subunit L2 of the Keanakākoʻi Tephra (Swanson and Houghton, 2019) is a deposit of hair resembling the modern hair deposits that formed in 2008–2018 and are understood to have had a similar origin from open-vent spattering, likely from a lava lake. In general, any lava lake with persistent spattering will produce abundant Pele's hair; a recent example at the time of writing is the Masaya lava lake in Nicaragua (Global Volcanism Program, 2025).

Figure 9. Photographs of distant and close views of Pele's hair. *A*, View of Pele's hair facing the sun, 1.5 kilometers (km) south of the lava lake at the summit of Kīlauea. Floor of topographic caldera of Kīlauea in background. Photograph taken July 29, 2013. *B*, Close-up of Pele's hair in drift 5 km southwest of the lava lake, taken November 16, 2012. *C*, Close-up of Pele's hair in drift 1 km south of lava lake, taken November 16, 2016; coin is 18 millimeters in diameter. All photographs taken by Don Swanson, U.S. Geological Survey.

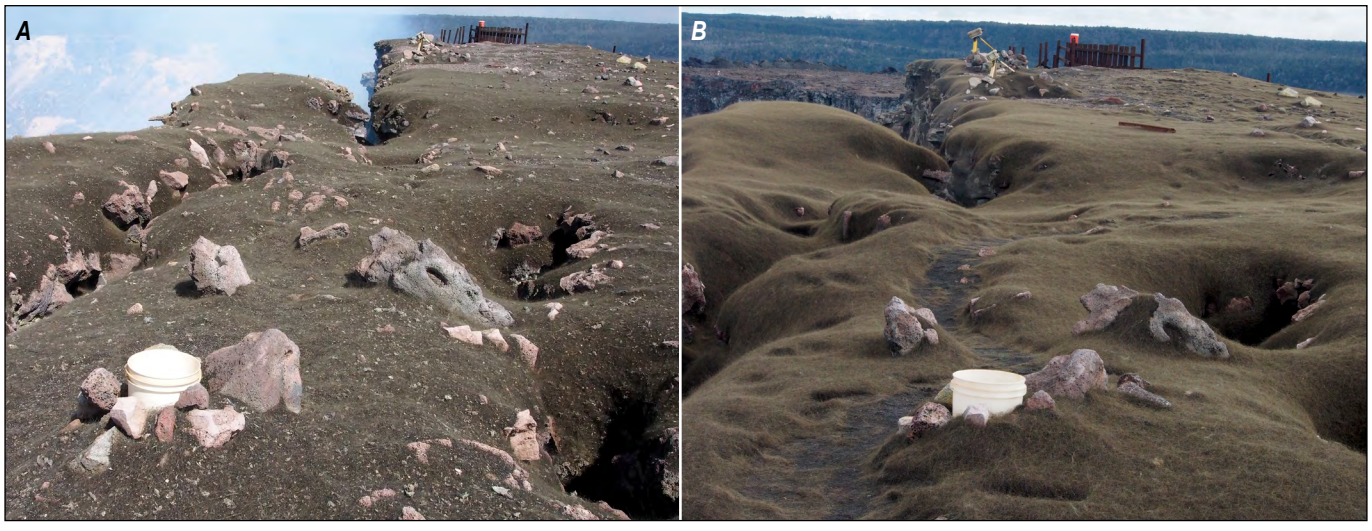

Figure 10. Photographs of Pele's hair. *A*, Accumulation of Pele's hair captured on November 9, 2016. *B*, Accumulation of Pele's hair captured on January 10, 2018, which was a time of rapid accumulation. White bucket in the foreground of both photographs is A7, and the bucket on the fence in the background is A8A. Photographs by Don Swanson, U.S. Geological Survey.

Size and Timing of the Explosive Events

Most of the 32 explosive events during the 10-year-long eruption were recognized on HVO webcams and are described in the narrative of the eruption (Patrick and others, 2021; chap. A of this volume). All these events left accumulations of tephra in the buckets that were higher than normal, and most made an identifiable deposit on the ground between buckets (fig. 11). In addition, webcam imagery shows many other rockfall-induced explosive events that were too small to send tephra coarser than medium ash onto the rim of Halema‘uma‘u.

Separate m/a and isomass maps were prepared for 24 out of 32 explosive events, using bucket accumulations or a combination of those accumulations with m/a measurements of the deposit between and beyond the buckets. The m/a values were contoured, and the bulk volume was estimated from the isomass contours by the method of Pyle (1989) using a deposit density of 1,300 kg/m^3. The results indicate that erupted bulk volumes range from 1 cubic meter (m^3) to 301 m^3, equivalent to values of the volcanic explosivity index (VEI) of −2 to −4 using the expanded VEI scale of Houghton and others (2013), which considers small eruptions not covered by the original VEI scale. No VEI was calculated for eight small explosions because subsequent tephra fall into the buckets contaminated that from the explosions themselves.

Three of the four largest explosions, with VEI of −2, occurred in 2008 (table 1). The first opened the eruption and contained no juvenile components (table 1; Houghton and others, 2011). The other two carried some juvenile clasts, with the September 2, 2008, event dominated by pumiceous lapilli. The fourth VEI −2 explosion took place on May 9, 2018, one day before the lava lake disappeared (fig. 12). The deposit of this explosion could not be studied adequately because of its timing, but it clearly resulted from the largest magmatic explosion of the eruption (table 1).

Most explosions had a juvenile content greater than 60 percent, but five explosions in 2008 and two in 2011 had fewer juvenile components (table 1; fig. 13). These seven exceptions took place when the lava lake was small and deep. Since 2008, the proportion of juvenile to non-juvenile (wall rock and secondary minerals) components showed no consistent change with time. Most of the post-2008 explosive events contained overwhelmingly juvenile components; 13 events had more than 90 percent juvenile material, as determined from componentry observations of tephra in buckets, and 6 of those 13 events had 95 percent or more juvenile material.

With an exception for 2008 and 2016, the explosive events were evenly distributed in time with little clustering (fig. 13). There were, however, eight explosions in 2008 and nine explosions in 2016. Why were 2008 and 2016 so different in terms of explosion timing?

In 2008, the vent in the Overlook crater was small and easily choked by rock falls, which could partly dam escaping magmatic gas. The March 19, 2008 event is a classic example of an explosion driven by magmatic gas but carrying no juvenile clasts (Houghton and others, 2011). Throughout the year, juvenile clasts progressively became more abundant (table 1; figs. 6, 13), but the vent remained small with the lava hidden from view for most of the time.

Figure 11. Photographs of deposits from the explosive event on April 28, 2015. *A*, Deposit in remains of visitor overlook that was abandoned in 2008. Blue bucket A8A is on the far corner of fence. White bucket A8 is toward the left edge of the photograph. *B*, Spatter clot, with rare vitreous surface, embedded in a clot with dull surface. Spatter with dull surfaces is studded with lithic grains mostly absent in vitreous clots. Scale in centimeters. The clot rests on lithic-rich ash from 2008. *C*, Spatter clot molded to fencing, with charred railing above. Photographs taken by Don Swanson, U.S. Geological Survey.

Figure 12. Photograph of eruption column on May 9, 2018, at Kīlauea, the last explosion before the lava lake disappeared. About 95 percent of the ejecta were juvenile, including pumice lapilli and small bombs. The explosion was triggered by a rockfall as the draining lava removed lateral support for the crater wall. Photograph by Gail Ferguson, U.S. Geological Survey.

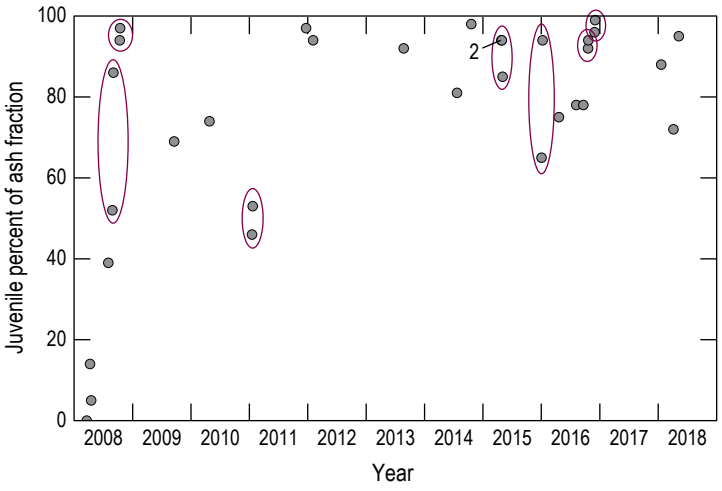

Figure 13. Plot showing percentage of juvenile components in 32 rockfall-induced explosive events of the 2008–2018 Kīlauea eruption. Ovals indicate events within 6 days of one another. In 2015, three events occurred within 8 days of one another. The number 2 indicates two events obscured by symbol size.

In contrast to 2008, the lake level was higher in 2016 than it had ever been before. Consequently, the site of explosions was closer to the Halemaʻumaʻu rim than previously, so the ejecta had less distance to travel to reach the rim. In other words, explosions that were weaker than in the past could nonetheless deposit ejecta outside Halemaʻumaʻu. In addition, parts of the crater wall that had previously been affected only slightly when the lake level was low now experienced prolonged heat and acidic gas. The wall responded by frequently shedding rock falls, nine of which resulted in spatter reaching the rim of Halemaʻumaʻu. These rock falls had no discernible influence on the near-daily tephra output before or after them, either in amount or juvenile percentage (fig. 6). The lake level was equally high for most of 2017, but by now the crater wall had equilibrated with the lake, and there were no explosive events because the rock falls were smaller and less frequent.

Some of the explosive events were clustered in time (table 1; fig. 13). Fifteen events took place within six days of one another, and three events happened within eight days in 2015. A likely explanation for the clustering is that a rockfall large enough to trigger one explosion could destabilize other parts of the crater wall, particularly those adjacent to the area of the first fall, leading to subsequent events in a short time span. The observation that 15 of the 32 events occurred within 6 days of one another became useful when assessing future rockfall-induced events.

April 16, 2008, Explosion

An explosion at 0236 Hawaii-Aleutian standard time (HST) on April 16, 2008, differed from all the other explosive events in componentry and dispersal characteristics. It produced a fine pink ash that was advected west-southwest from the Overlook crater, a direction different from the prevalent south-southwest direction (figs. 14, 15; Houghton and others, 2013). An anemometer, an instrument that measures wind speed and direction, at HVO recorded a northeast wind direction of about 50 degrees with a speed of 2.5 m/s at the time of the April 16 eruption. This wind direction was roughly consistent with the dispersal direction of the ash. The dispersed ash avoided most of the bucket network, but its axis was almost exactly along Crater Rim Drive on the Kīlauea caldera floor, so that the deposit could be readily accessed and examined. During daylight on April 16, m/a measurements were made at 26 locations along the paved

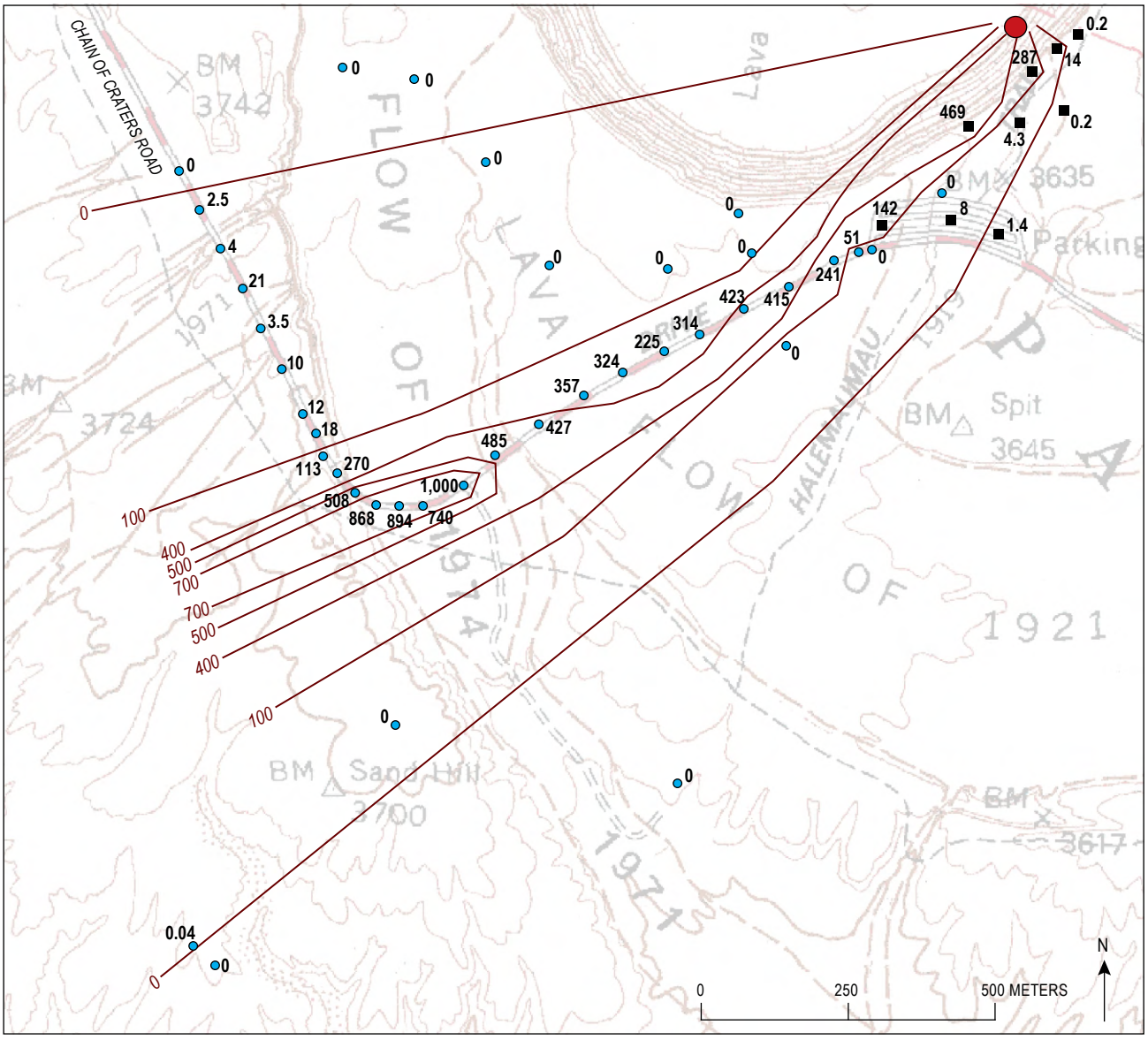

Base from U.S. Geological Survey, Kilauea Crater, 1:24,000, 1981

EXPLANATION

- Isomass line
- Overlook Crater
- Mass per unit area measurement locations
- Mass per unit area measurement at buckets A1–A9

Figure 14. Map showing mass per unit area (m/a) measurements of ash erupted at 0236 Hawaii-Aleutian standard time on April 16, 2008. Values in grams per square meter (g/m^2). Isomass contours are at 0, 100, 400, 500, and 700 g/m^2. Note the narrow dispersal for the m/a values >100 g/m^2. The margin of the deposit (the 0 isopleth) is uncertain, because thin ash was hard to identify off the paved road.

Figure 15. Photograph of pink, mostly lithic ash on caldera floor, erupted at 0236 Hawaii-Aleutian standard time (HST) April 16, 2008. Photograph taken at 0718 HST April 17, 2008. The 1-square-meter area to the right of the photograph was scraped free of ash on April 16 for mass per unit area (m/a) measurement. Photograph taken by Don Swanson, U.S. Geological Survey.

road, as well as at 13 locations off the road, where the thin ash was difficult to recognize. In a day or two, rain had removed much of the deposit.

The m/a measurements clearly indicated a closed-contour maximum isomass value of about 1,000 grams per square meter (g/m^2) located about 1,200 m from the Overlook crater (fig. 14). At that distance, the 100 g/m^2 isomass contour was only about 150 m from the 1,000 g/m^2 contour in a direction normal to the dispersal axis. The ash was hard to detect off the pavement, but measurements along the paved road showed that the northern edge of the deposit was about 650 m north of the dispersal axis. Attempts to define the precise edge of the fall deposit were unsuccessful; figure 14 shows locations where we think the ash was absent. The complex isomass contours, with the maximum so far from the vent, made it impossible to apply the method of Pyle (1989) to estimate volume. Consequently, we were not able to calculate a VEI.

The deposit, which was wet when measured, was fine, slippery, and contained few clasts >1 mm in diameter, even in the proximal buckets A1, A4, and A7. The pink color was distinctive; no other explosion during the eruption produced a deposit that was as fine or colorful.

Componentry examination of the April 16 explosion indicated that only about 5 percent of the ash was juvenile. The rest consisted of altered wall rock. The combination of the fine grain size and the altered nature of the ejecta indicates that an area of secondary alteration on the crater wall was the source of most of the ejecta.

Conclusion

Frequent collection of tephra from the bucket network allowed recognition and interpretation of long-term trends in accumulation, which therefore allowed understanding of eruption, rate, dispersal characteristics, and changes in componentry of Halemaʻumaʻu. The near-daily collection routine provided samples of the lava lake not obtainable by other means; these samples, although typically small, can be used to provide a detailed version of changing lava composition. If a long-lasting lava lake returns to Halemaʻumaʻu, as is almost certain in the future, establishment of a similar tephra collection network could be beneficial. This is something that cannot be done remotely, and the near-daily visit to the network afforded a way for geologists to maintain a close visual and audible connection to the entire lava lake that supplemented the fixed-view camera observations from webcams. Routine tephra sampling remains a part of every eruption study, and the 2008–2018 eruption in the Overlook crater provided an unparalleled opportunity to put this field-oriented thinking into practice.

Each volcano is different, and the procedures we used were geared to the easily accessible Halemaʻumaʻu. Our study benefited from closely spaced collecting sites because the goal is to sample tephra within a few hundred meters of the vent. More distally, collectors can be widely spaced, but the details of vent configuration and depth affect tephra production and accumulation in the near-field environment.

References Cited

Carey, R.J., Swavely, L., Swanson, D.A., Houghton, B.F., Orr, T.R., Elias, T., and Sutton, A.J., 2015, Onset of a basaltic explosive eruption from Kīlauea's summit in 2008, chap. 19 *of* Carey, R., Cayol, V., Poland, M., and Weis, D., eds., Hawaiian Volcanoes—From Source to Surface: American Geophysical Union Geophysical Monograph, v. 208, p. 421–437, https://doi.org/10.1002/9781118872079.ch19.

Eychenne, J., Houghton, B.F., Swanson, D.A., Carey, R.J., and Swavely, L., 2015, Dynamics of an open basaltic magma system—The 2008 activity of the Halema'uma'u Overlook vent, Kīlauea Caldera: Earth and Planetary Science Letters, v. 409, p. 49–60, https://doi.org/10.1016/j.epsl.2014.10.045.

Global Volcanism Program, 2025, Masaya (344100), *in* Volcanoes of the World (ver. 5.3.0, July 2025), Venzke, E., ed.: Smithsonian Institution database, accessed March 19, 2026, at https://volcano.si.edu/volcano.cfm?vn=344100.

Houghton, B.F., Swanson, D.A., Biass, S., Fagents, S.A., and Orr, T.R., 2017, Partitioning of pyroclasts between ballistic transport and a convective plume—Kīlauea volcano, 19 March 2008: Journal of Geophysical Research. Solid Earth, v. 122, no. 5, p. 3379–3391, https://doi.org/10.1002/2017JB014040.

Houghton, B.F., Swanson, D.A., Carey, R.J., Rausch, J., and Sutton, A.J., 2011, Pigeonholing pyroclasts—Insights from the 19 March 2008 explosive eruption of Kīlauea volcano: Geology, v. 39, no. 3, p. 263–266, https://doi.org/10.1130/G31509.1.

Houghton, B.F., Swanson, D.A., Rausch, J., Carey, R.J., Fagents, S.A., and Orr, T.R., 2013, Pushing the Volcanic Explosivity Index to its limit and beyond—Constraints from exceptionally weak explosive eruptions at Kīlauea in 2008: Geology, v. 41, no. 6, p. 627–630, https://doi.org/10.1130/G34146.1.

Mintz, B.G., Houghton, B.F., Llewellin, E.W., Orr, T.R., Taddeucci, J., Carey, R.J., Kueppers, U., Gaudin, D., Patrick, M.R., Burton, M., Scalato, P., and La Spina, A., 2021, Patterns of bubble bursting and weak explosive activity in an active lava lake—Halema'uma'u, Kīlauea, 2015, chap. E *of* Patrick, M., Orr, T., Swanson, D., and Houghton, B., eds., The 2008–2018 summit lava lake at Kīlauea Volcano, Hawai'i: U.S. Geological Survey Professional Paper 1867, 16 p., https://doi.org/10.3133/pp1867E.

Mueller, S.B., Houghton, B.F., Swanson, D.A., Fagents, S.A., and Klawonn, M., 2018, Intricate episodic growth of a Hawaiian tephra deposit—Case study of the 1959 Kīlauea Iki eruption: Bulletin of Volcanology, v. 80, no. 10, p. 73, https://doi.org/10.1007/s00445-018-1249-6.

Orr, T.R., Thelen, W.A., Patrick, M.R., Swanson, D.A., and Wilson, D.C., 2013, Explosive eruptions triggered by rockfalls at Kīlauea volcano, Hawai'i: Geology, v. 41, no. 2, p. 207–210, https://doi.org/10.1130/G33564.1.

Patrick, M., Orr, T., Swanson, D., Houghton, B., Wooten, K., Desmither, L., Parcheta, C., and Fee, D., 2021, Kīlauea's 2008–2018 summit lava lake—Chronology and eruption insights, chap. A *of* Patrick, M., Orr, T., Swanson, D., and Houghton, B., eds., The 2008–2018 summit lava lake at Kīlauea Volcano, Hawai'i: U.S. Geological Survey Professional Paper 1867, 50 p., https://doi.org/10.3133/pp1867A.

Pyle, D.M., 1989, The thickness, volume and grainsize of tephra fall deposits: Bulletin of Volcanology, v. 51, no. 1, p. 1–15, https://doi.org/10.1007/BF01086757.

Shimano, T., Nishimura, T., Chiga, N., Shibasaki, Y., Iguchi, M., Miki, D., and Yokoo, A., 2013, Development of an automatic volcanic ash sampling apparatus for active volcanoes: Bulletin of Volcanology, v. 75, no. 12, p. 773, https://doi.org/10.1007/s00445-013-0773-7.

Swanson, D.A., and Houghton, B.F., 2019, Products, processes, and implications of Keanakāko'i volcanism, Kīlauea Volcano, Hawai'i, *in* Poland, M.P., Garcia, M.O., Camp, V.E., and Grunder, A., eds., Field Volcanology—A Tribute to the Distinguished Career of Don Swanson: Geological Society of America Special Paper, v. 538, p. 159–190, https://doi.org/10.1130/2018.2538(07).

Swanson, D.A., Orr, T.R., Patrick, M.R., and Houghton, B.F., 2026, Tephra accumulation and wind data for Kīlauea's 2008–2018 lava lake eruption: U.S. Geological Survey data release, https://doi.org/10.5066/P144UD4G.

Swanson, D.A., Patrick, M.R., and Orr, T.R., 2017, Slowly pulsing magma supply inferred from changes in level of the lava lake in Overlook crater, Kīlauea [abs.] *in* International Association of Volcanology and Chemistry of the Earth's Interior [IAVCEI], Portland, Oreg., August 14–18, 2017: IAVCEI, abstract no. 1074.

Swanson, D., Wooten, K., and Orr, T., 2009, Buckets of ash track tephra flux from Halema'uma'u Crater, Hawai'i: Eos (Washington, D.C.), v. 90, no. 46, p. 427, https://doi.org/10.1029/2009EO460003.

Wooten, K.M., Thornber, C.R., Orr, T.R., Ellis, J.F., and Trusdell, F.A., 2009, Catalog of tephra samples from Kīlauea's summit eruption, March–December 2008: U.S. Geological Survey Open-File Report 2009–1134, 26 p., https://doi.org/10.3133/ofr20091134.

Moffett Field Publishing Science Center, California
Manuscript approved May 14, 2026
Edited by Hayden Chaisson
Layout and illustration support by Cory Hurd

ISSN 2330-7102 (online)
https://doi.org/10.3133/pp1867D